(Received 17 November 2025, Accepted 11 December 2025, Scheduled 6 February 2026)

Design of a Flexible and Tri-Band MIMO Antenna for Conformal Wi-Fi 7/5G Applications

Tian-Xiang Wang, Cheng-Zhu Du*, and Xi Sun

College of Electronics and Information Engineering, Shanghai University of Electric Power, Shanghai 200090, China

ABSTRACT: This paper describes a flexible dual-port multiple-input multiple-output (MIMO) antenna system tailored for multi-band operation, covering 2.4 GHz Wi-Fi, 3.5 GHz 5G, as well as the 5–7 GHz band used in wireless applications such as Wi-Fi 7. The antenna is fabricated on a liquid crystal polymer (LCP) substrate, featuring an ultra-thin profile of 0.1 mm and a compact size of $60 \times 35\,\text{mm}^2$, making it highly suitable for integration into modern flexible and wearable devices. To achieve high port isolation, a complementary split-ring resonator (CSRR) structure is incorporated between the two radiating elements. The measurement results indicate that the antenna achieves impedance bandwidths across 1.36–2.71 GHz, 3.07–3.655 GHz, and 4.015–8.245 GHz, which fully cover the target frequency bands of 2.4–2.483 GHz, 3.4–3.5 GHz, and 5.15–7.125 GHz. The antenna's performance is comprehensively characterized by evaluating key parameters, including S-parameters, envelope correlation coefficient (ECC), diversity gain (DG), total active reflection coefficient (TARC), gain, mean effective gain (MEG), and radiation patterns, along with other relevant metrics. All measured results confirm that the antenna meets the essential requirements for MIMO and diversity systems. Furthermore, bending tests conducted at two distinct radii of 30 mm and 50 mm confirm stable antenna performance, verifying its mechanical robustness and reliability under practical bending conditions.

1. INTRODUCTION

The relentless evolution of wireless communication systems — encompassing Wi-Fi standards (including the latest Wi-Fi 7), 5G, and the emerging 6G — has driven an unprecedented demand for multi-band capable, high-speed, and compact mobile devices [1–5]. These technologies operate across several key frequency bands, most notably the 2.4 GHz ISM band, 5G sub-6 GHz band spanning 3.4 to 3.6 GHz, and 5–7 GHz range, which is crucial for Wi-Fi 6E and future applications, requiring antennas to support broad bandwidths and seamless multi-standard operation. Concurrently, the emergence of flexible electronics for applications in wearable devices, biomedical sensors, and conformal systems has driven the need for antennas that are not only electromagnetically proficient but also mechanically robust and adaptable [6–8]. Hence, many flexible antennas have been printed on the flexible substrates. Among various substrate candidates, liquid crystal polymer (LCP) stands out due to its exceptional properties, such as a low and stable dielectric constant, extremely low moisture absorption, and a compatible coefficient of thermal expansion, making it an ideal substrate for fabricating high-performance, flexible microwave components and antennas [9–11]. Furthermore, to meet the escalating requirements aimed at augmenting channel capacity and strengthening link reliability within the confines of limited space, multiple-input multiple-output (MIMO) technology has been adopted as a cornerstone of modern communication standards, leveraging multiple antenna elements to dramatically enhance data throughput and mitigate multipath fading.

MIMO technology is a fundamental paradigm for enhancing channel capacity and link reliability without requiring additional spectrum, leveraging spatial multiplexing to increase data rates and combat multipath fading [12]. However, integrating multiple antenna elements within the compact form factors of modern devices introduces significant mutual coupling, which degrades impedance matching, radiation efficiency, and overall MIMO performance [13]. To mitigate this issue, various decoupling techniques have been developed. They include defected ground structures (DGS) [14–16] that disrupt surface currents, electromagnetic band-gap (EBG) [17–19] structures that suppress surface waves, neutral lines (NL) [20, 21] that cancel coupling currents, and complementary split-ring resonators (CSRRs) [22, 23] which provide resonant isolation — each offering distinct mechanisms to achieve high port isolation in multi-antenna systems.

With the development of flexible and wearable technology, many wearable antennas have been proposed [24–28], particularly those capable of supporting multi-band and multi-port MIMO operations. For instance, the flexible antenna in [24] achieves triple-band operation (covering 2.28–2.56 GHz, 3.28–3.85 GHz, and 5.06–7.30 GHz) but is limited to a single antenna element. Conversely, the design in [25] implements a two-port MIMO configuration on a flexible substrate; however, it only supports dual-band operation (2.15–2.87 GHz and 5.13–5.86 GHz), lacking broader coverage. In pursuit of higher channel capacity, significant efforts have been devoted to developing flexible MIMO systems with more antenna ports, as seen

* Corresponding author: Chengzhu Du (duchengzhu@163.com).

in the four-element designs of [26–28]. Nevertheless, these designs often cover a limited number of bands or narrower bandwidths (e.g., [26] covering 3.33–3.89 GHz, [27] covering 3.05–3.74 GHz). Another flexible four-port MIMO antenna in [28] offers dual-band operation (3.156–3.84 GHz and 4.638–6.348 GHz), yet a wider continuous bandwidth covering key bands like 2.4 GHz and the entire 5–7 GHz range is highly desirable for comprehensive multi-standard applications. So, the antenna achieving both multi-band operation and multi-port MIMO configuration within a compact flexible structure remains challenging.

In this paper, a miniaturized two-element flexible MIMO antenna array fabricated on a liquid crystal polymer (LCP) substrate is developed to achieve multi-band operation, covering the frequency ranges of 2.4–2.483 GHz, 3.4–3.5 GHz, and 5.15–7.125 GHz, which are essential for Wi-Fi 7 and 5G wireless systems. To mitigate the mutual coupling typically encountered in tightly arranged MIMO configurations, a CSRR is incorporated into the shared ground plane. This technique is chosen due to its demonstrated efficiency, straightforward implementation, and negligible influence on the antenna's physical dimensions, an essential factor for flexible electronics. The fabricated MIMO antenna achieves a measured port isolation exceeding 20 dB across all target bands.

2. ANTENNA DESIGN

2.1. Single Element Antenna

A 0.1 mm-thick LCP substrate, with a dielectric constant of 2.9 and a loss tangent of 0.002, serves as the platform for the proposed antenna. Figure 1 shows the geometry of the antenna element, which is fed by a coplanar waveguide (CPW).

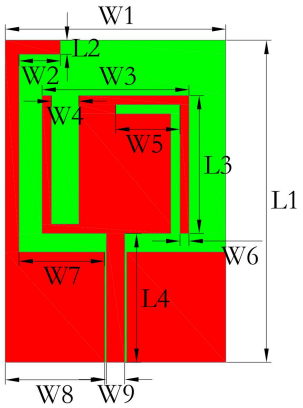

FIGURE 1. Unit antenna geometry.

The detailed geometric dimensions (in mm) are as follows: $W1 = 24$, $L1 = 35$, $W2 = 4.5$, $W3 = 16$, $W4 = 3$, $W5 = 6$, $W6 = 1$, $W7 = 9.3$, $W8 = 10.8$, $W9 = 2$, $L2 = 1.5$, $L3 = 15$, $L4 = 14$.

The progressive design stages of the antenna element, along with their corresponding performance outcomes, are depicted in Figure 2. The initial structure (Step 1) employs a CPW-fed configuration, consisting of a rectangular radiating patch and a pair of symmetrical metal ground planes. This rectangular

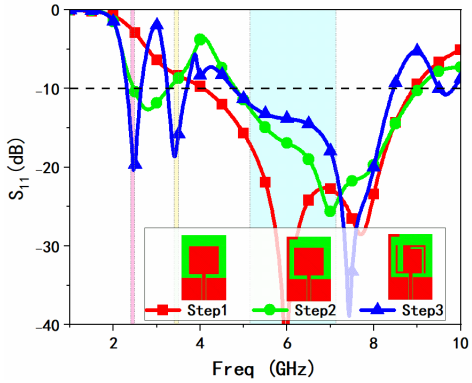

FIGURE 2. Evolution of the antenna element design and its performance.

patch is primarily responsible for exciting the fundamental operating band at 4.08–8.92 GHz. To enhance low-frequency performance, Step 2 incorporates an "L"-shaped stub into one of the ground planes. Finally, based on Step 2, an "I"-shaped slot and an "L"-shaped slot are etched onto the radiating patch to form the Step 3 structure. This modification not only shifts the lower resonance downward to around 2.4 GHz but also successfully generates an additional resonant mode within the range of 3.24–3.68 GHz.

To further investigate the influence of key structural parameters on the operating bandwidth of the antenna, a detailed parametric analysis of the connecting structure parameter $W5$ was carried out, with the results presented in Figure 3. The analysis indicates that the antenna's low-frequency performance is highly sensitive to variations in $W5$. As the length of $W5$ increases, the bandwidth around 2.45 GHz gradually narrows, while the bandwidth near 3.45 GHz correspondingly expands. When $W5$ is set to 7 mm, the antenna exhibits optimal overall radiation performance across all bands, identifying this dimension as the best design parameter for achieving superior performance.

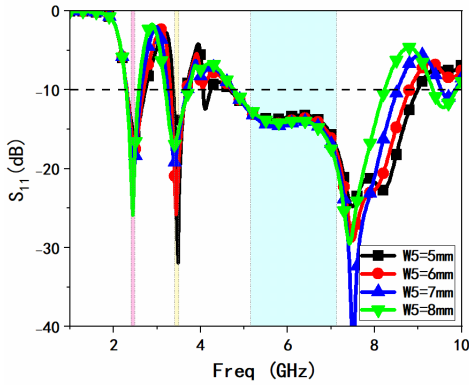

FIGURE 3. Parametric analysis of $W5$.

2.2. Two-Element MIMO Antenna

To construct a dual-element MIMO antenna system, dual-port antennas were arranged in an array with a symmetrical layout in this study, and an additional isolation optimization structure was introduced to suppress the electromagnetic coupling be-

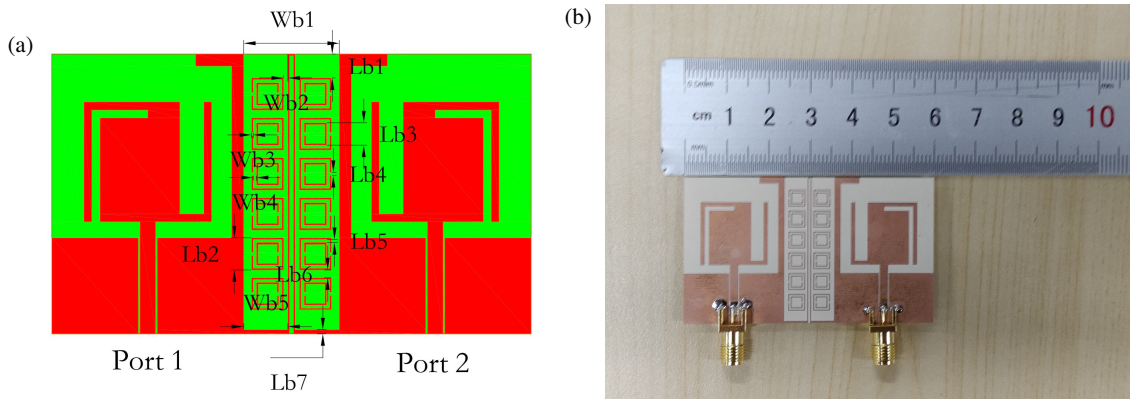

FIGURE 4. Dimension and physical drawing of binary: (a) Antenna geometry; (b) Fabricated antenna prototype.

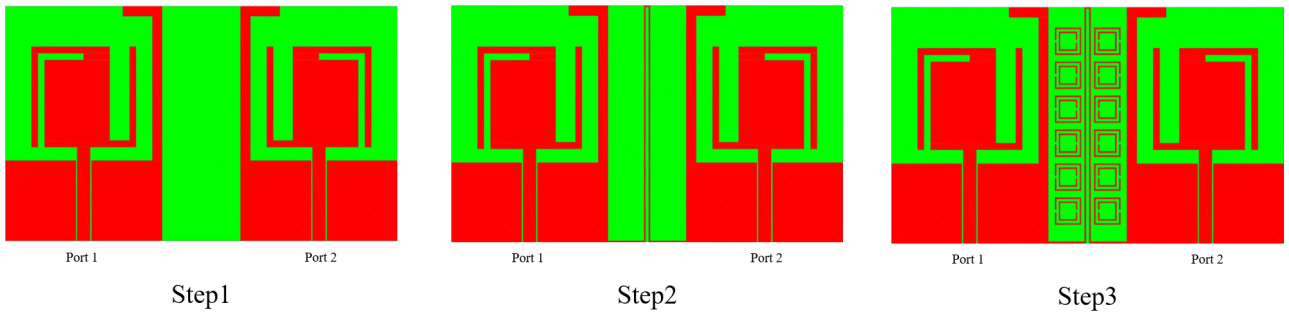

FIGURE 5. Evolution of 2-port antenna.

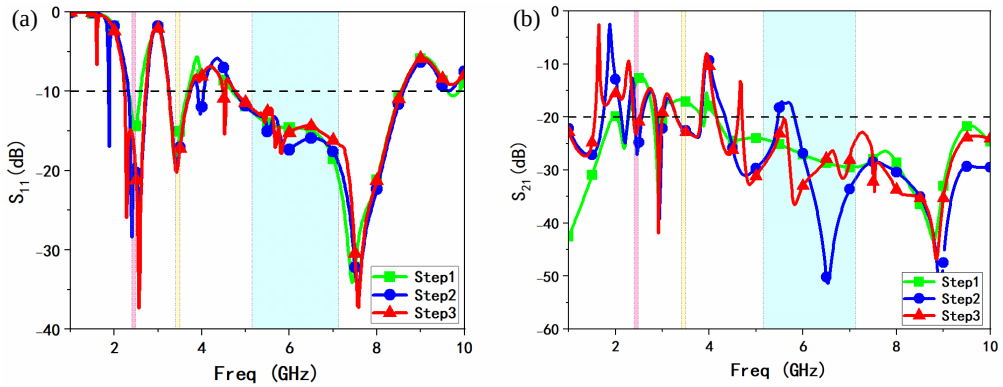

FIGURE 6. S-parameters of Step 1–Step 3: (a) Reflection coefficient; (b) Isolation.

tween the elements. Based on the above design scheme, the structural diagram of the resulting dual-element MIMO antenna is shown in Figure 4(a); meanwhile, to verify the feasibility of the design, the physical fabrication of the antenna has been completed, and its physical photograph is presented in Figure 4(b).

The detailed geometric dimensions (in mm) are as follows: $Wb1 = 12$, $Wb2 = 0.55$, $Wb3 = 0.2$, $Wb4 = 0.4$, $Wb5 = 5.55$, $Lb1 = 3$, $Lb2 = 4$, $Lb3 = 2.8$, $Lb4 = 0.4$ mm, $Lb5 = 0.4$, $Lb6 = 1$, $Lb7 = 0.5$.

Figure 5 presents the structural evolution of the two-element antenna. Figure 6 illustrates the corresponding S-parameter variations at each design step.

In Step 1, the initial configuration is formed by placing two antenna elements symmetrically. In Step 2, the ground of two antenna elements are connected by a branch, which improves the isolation at 2.45 GHz and 3.45 GHz, and the isolation is only better than 17 dB within the 5.48–5.84 GHz band. Finally, in Step 3, twelve CSRR structures are symmetrically arranged along the central ground plane by parametric sweeping and empirical selection, and the isolation is better than 20 dB at all working bands, effectively enhancing the isolation across the 5.15–7.125 GHz frequency range. The suppression frequency of the CSRR is primarily governed by its equivalent electrical length. In this design, the total conductor length of the outer ring arm of each CSRR is 15.6 mm, which is close to a quarter-wavelength at 5.5 GHz ($\lambda_0/4 \approx 13.6$ mm).

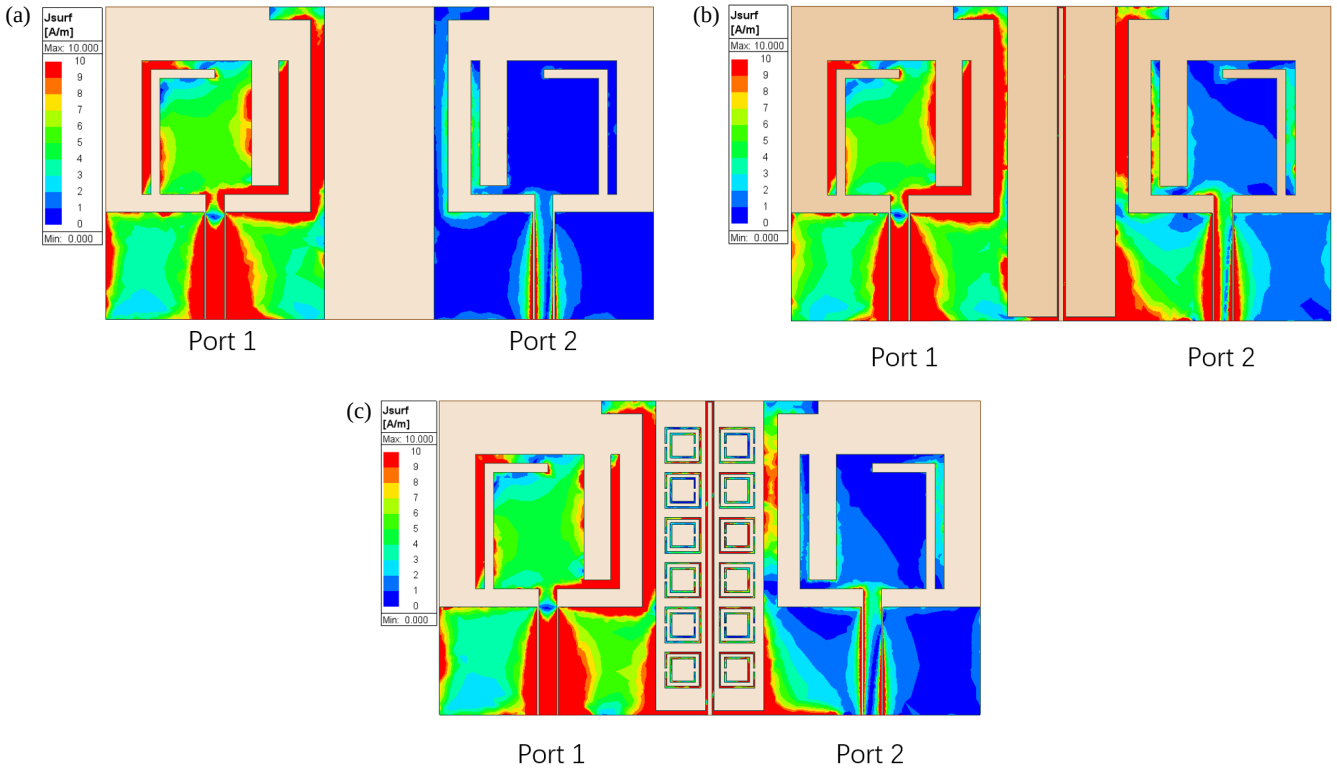

FIGURE 7. Current distribution: (a) Step 1; (b) Step 2; (c) Step 3.

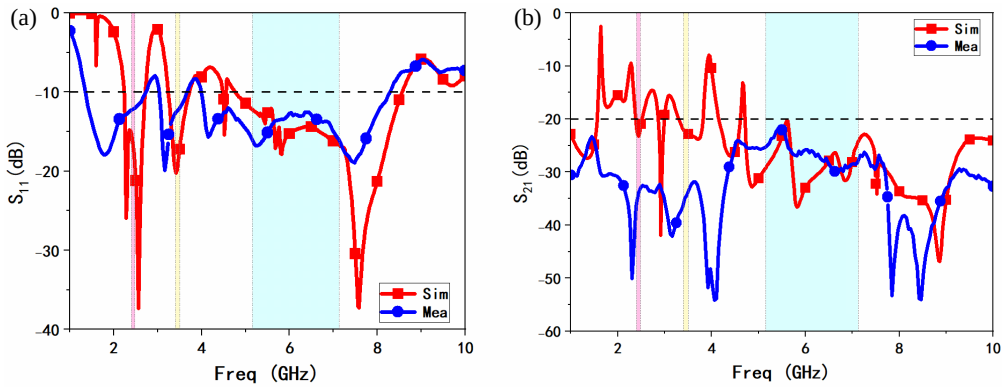

FIGURE 8. Comparison of the simulated and measured S-parameters of the antenna: (a) Reflection coefficient; (b) Isolation.

2.3. Decoupling Structure Analysis

Figure 7 presents the simulated current distribution of the antenna at 5.6 GHz under the condition of exciting Port 1 and terminating Port 2 with a 50-Ohm load. In Step 1, without any isolation structure, relatively weak coupling current is observed near Port 2. In Step 2, after connecting the two antenna elements, the coupling current becomes noticeable around the "L"-shaped stub. In Step 3, with the introduction of a CSRR structure, strong coupling current is concentrated around the CSRR unit, and the current amplitude at Port 2 is significantly suppressed. These results demonstrate that the port isolation is effectively improved by adding a CSRR structure at 5.6 GHz bands.

3. MEASURED RESULTS AND ANALYSIS

3.1. S-Parameters

The measured S-parameters of the fabricated antenna, as shown in Figure 8, demonstrate that the proposed two-element MIMO antenna operates across three frequency bands: 1.36–2.71 GHz, 3.07–3.655 GHz, and 4.015–8.245 GHz, which satisfactorily meet the design specifications. Furthermore, the port isolation exceeds 20 dB across the entire operating range. Some minor discrepancies are noted between the measured and simulated data, primarily due to practical imperfections such as soldering quality and the measurement environment.

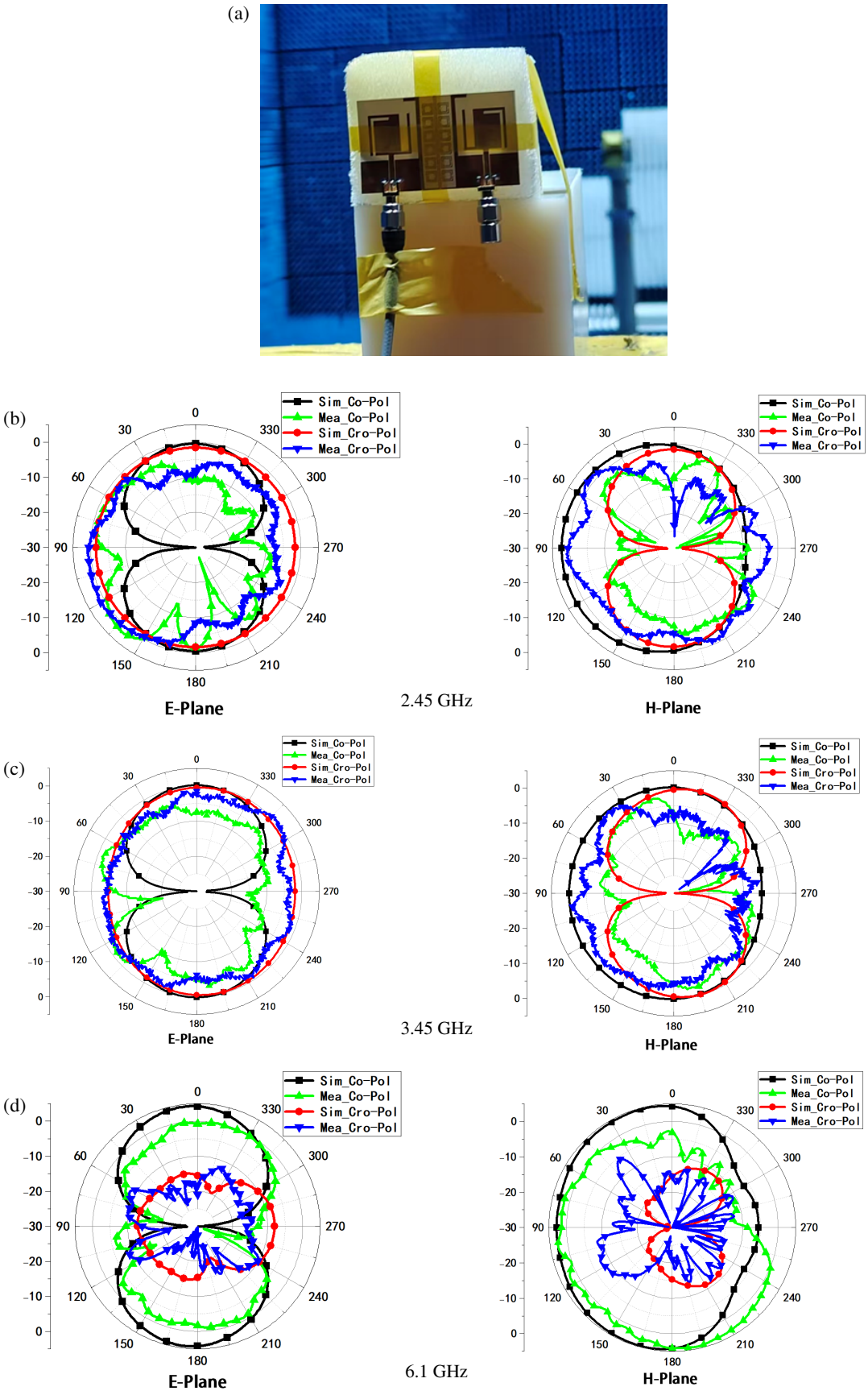

FIGURE 9. Characterization of radiation patterns: (a) Radiation pattern measurement environment; (b) 2.45 GHz; (c) 3.45 GHz; (d) 6.1 GHz.

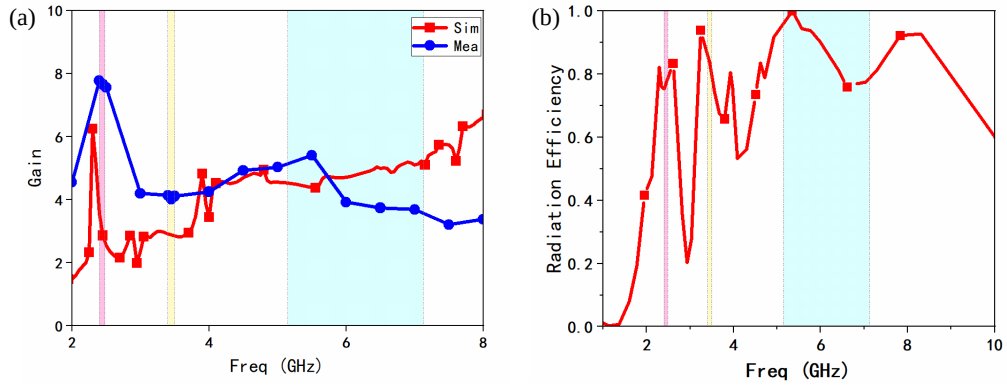

FIGURE 10. Gain and radiation efficiency: (a) Gain; (b) Simulated radiation efficiency.

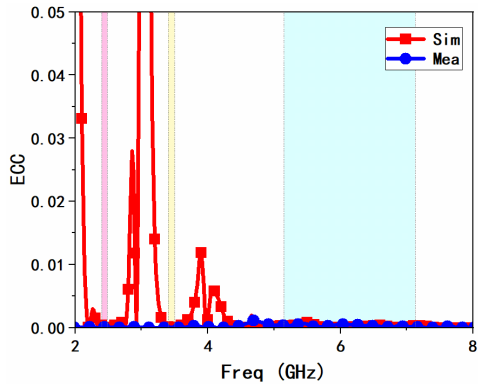

FIGURE 11. ECC of the proposed antenna.

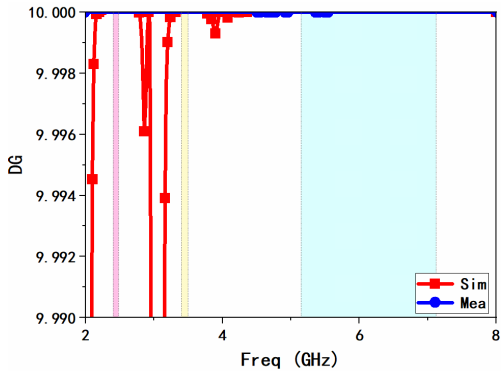

FIGURE 12. DG of the proposed antenna.

3.2. Radiation Patterns

Figure 9 depicts the E- and H-plane radiation patterns of the two-element MIMO antenna at three principal operating frequencies: 2.45 GHz, 3.45 GHz, and 6.1 GHz, covering both co- and cross-polarization. At 2.45 GHz, the E-plane co-polarization pattern features a clear figure-eight form. In contrast, the H-plane pattern is largely omnidirectional, with the cross-polarization showing the opposite behavior. At the higher frequencies (3.45 and 6.1 GHz), notable variations are observed in the radiation intensity and beamwidth of the patterns for both polarizations across the two planes.

3.3. Gain and Radiation Efficiency

At 2.4 GHz, the antenna achieves a peak measured gain of 7.78 dB, as illustrated in Figure 10(a). Both measured and simulated gains remain above 2 dB across most of the frequency range, demonstrating favorable antenna performance. It can be observed that the measured gain is generally higher than the simulated result below 6 GHz, whereas above this frequency, the measured values become slightly lower. Such a discrepancy may be attributed to practical factors such as SMA connector effects, soldering quality, and the testing environment. Figure 10(b) shows the simulated radiation efficiency, and the radiation efficiency is above 74% for all operating bands.

3.4. Diversity Performance

The channel correlation between antennas is evaluated using the envelope correlation coefficient (ECC), a core parameter for quantifying the signal coupling degree between antennas. ECC is calculated based on the S-parameters of the antenna system, and its specific mathematical expression is given in Equation (1):

$$\rho_e(i,j,N) = \left| \frac{\sum_{n=1}^{N} S_{i,n}^{*} S_{n,j}}{\left| \prod_{k=i,j} \left(1 - \sum_{n=1}^{N} S_{k,n}^{*} S_{n,k}\right) \right|^{1/2}} \right|^2 \quad (1)$$

As illustrated in Figure 11, the measured ECC values of the antenna system remain below 0.0012 across the entire target operating band, which is significantly lower than the standard threshold of 0.5 in engineering applications. This result fully indicates that the signal coupling degree between the designed antenna elements is extremely low, endowing the system with excellent isolation performance and effectively avoiding signal interference between channels.

The diversity performance of the antenna system is quantitatively evaluated by the diversity gain (DG), a key parameter characterizing the diversity reception capability. DG has a clear theoretical correlation with ECC, and its mathematical derivation is provided in Equation (2):

$$DG = 10\sqrt{1 - (ECC)^2} \quad (2)$$

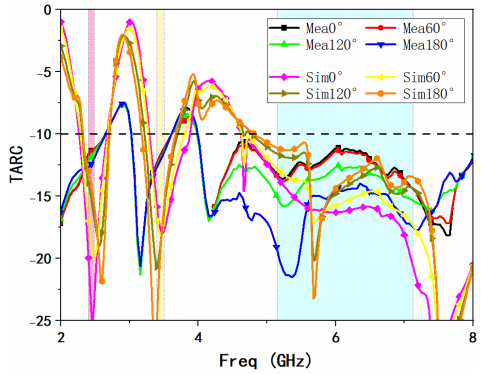

FIGURE 13. TARC of the antenna.

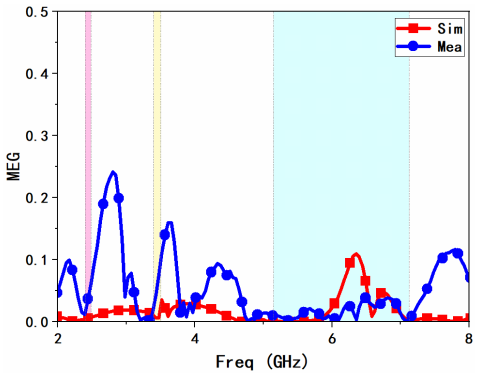

FIGURE 14. MEG.

As shown in the measured results of Figure 12, the measured DG values of the antenna system are all higher than 9.99999 dB throughout the operating band with minimal fluctuations. These results further verify that the designed antenna system can stably achieve efficient diversity reception, which significantly improves the reliability of signal reception in complex electromagnetic environments.

In the design of MIMO antenna systems, conventional S-parameters are only applicable under ideal conditions where a single port is excited, and the remaining ports are matched. They fail to accurately characterize the actual response when multiple ports operate simultaneously, thus presenting significant limitations in practical performance evaluation. To more comprehensively assess the compatibility and radiation efficiency of MIMO antennas under multi-port excitation, the total active reflection coefficient (TARC) must be introduced. Its mathematical expression is as follows:

$$TARC = N^{-0.5}\sqrt{\sum_{i=1}^{N}\left|\sum_{k=1}^{N} S_{ik}e^{j\theta_{k-1}}\right|^2} \tag{3}$$

where S_{ik} denotes the scattering parameter, θ the excitation phase difference among ports, and N the total number of antenna elements.

As shown in Figure 13, the TARC of this dual-element MIMO flexible antenna exhibits robust stability across the operating band when the excitation phase varies from 0° to 180° in 60° increments. Both simulated and measured curves remain below the -10 dB threshold throughout the target frequency band, meeting the practical requirements for radiation efficiency and impedance matching in multi-antenna systems.

The mean effective gain (MEG) is used to quantify the statistical characteristics of the received power of individual antenna elements in multipath environments within multi-antenna systems. The theoretical framework is defined by Equations (4) and (5):

$$MEG_i = 0.5\left[1 - \sum_{j=1}^{N}|S_{ij}|^2\right] \tag{4}$$

$$|MEG_i - MEG_j| < 3\,\text{dB} \tag{5}$$

where N denotes the total number of antenna elements. Engineering specifications require that the MEG variation between any two elements must remain below the 3 dB threshold.

As shown in Figure 14, a comparative assessment of the simulated and measured MEG performances is provided. Both simulated and measured results demonstrate that all inter-element MEG differences are rigorously constrained within 1 dB across the operational bandwidth, confirming the design's consistent performance in practical environments.

In an ideal MIMO antenna system, the channel capacity increases linearly with the number of antenna elements. However, in practical scenarios, mutual coupling among antenna elements leads to pattern distortion and increased channel correlation, significantly degrading the spatial multiplexing performance. To quantify this degradation, a key metric referred to as channel capacity loss (CCL) — defined as the difference between the ideal and the actual channel capacity — is introduced. This metric effectively captures the extent of capacity deterioration under realistic conditions. In engineering practice, it is generally required that CCL remains below 0.5 bps/Hz, indicating that the system performs near-ideally and can efficiently utilize MIMO spatial resources, thereby fully leveraging the advantages of the multi-antenna architecture.

The comparison between simulated and measured CCL characteristics over the antenna's operating bandwidth is depicted in Figure 15. All measured CLL values strictly adhere to the engineering threshold of 0.5 bps/Hz. This empirical validation

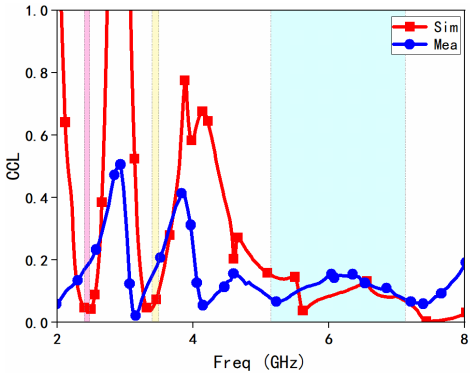

FIGURE 15. CCL.

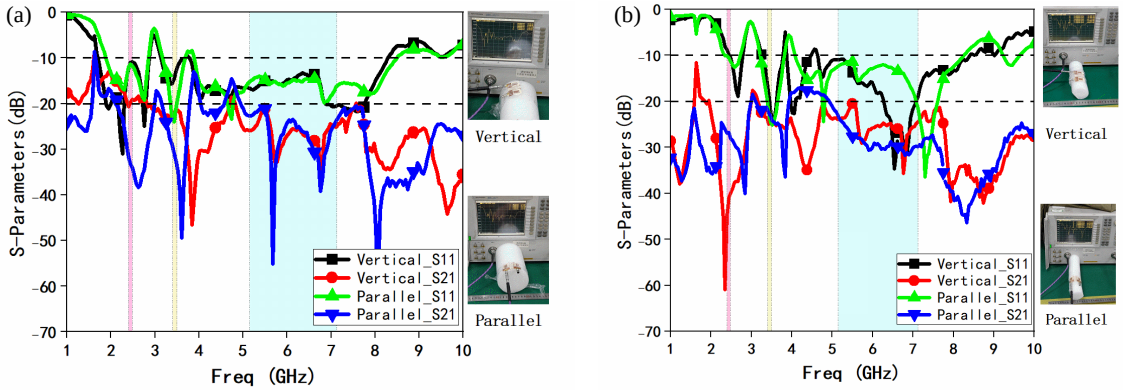

FIGURE 16. Reflection characteristics under bending conditions: (a) $R = 50$ mm, (b) $R = 30$ mm.

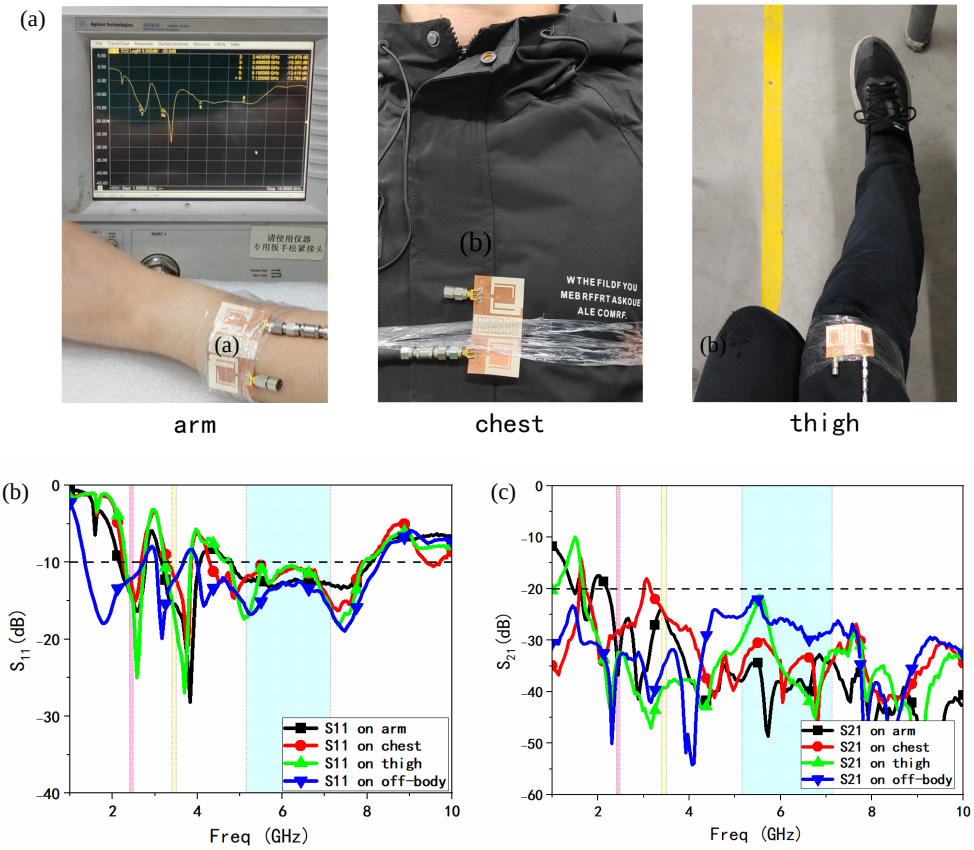

FIGURE 17. Comparison of S-parameters and measurement scenarios for the antenna at different on-body positions: (a) Antenna body measurement; (b) S_{11}; (c) S_{21}.

confirms the capability of the proposed antenna system to effectively suppress inter-channel interference.

3.5. Flexibility Analysis

Bending tests were conducted by conformally wrapping the flexible antenna onto 30 mm and 50 mm radius foam dielectric cylinders, with the feed line oriented both parallel and perpendicular to the cylinder axis. This study investigates the bending response of a two-element MIMO patch antenna, with particular focus on its S-parameters under each condition. As shown in Figure 16, when bent on the 50 mm radius cylinder, only the configuration with the feed line perpendicular to the axis exhibits a slight degradation in isolation, though it remains better than 19 dB; all other cases demonstrate excellent performance. Similarly, with the 30 mm radius cylinder, a minor decrease in performance is observed only when the feed line is perpendicular to the axis, while all other configurations maintain favorable performance, indicating robust bending adaptability.

3.6. Effects of Human Body

This section investigates the antenna's performance when it is worn on the human body. Tests were conducted by placing the

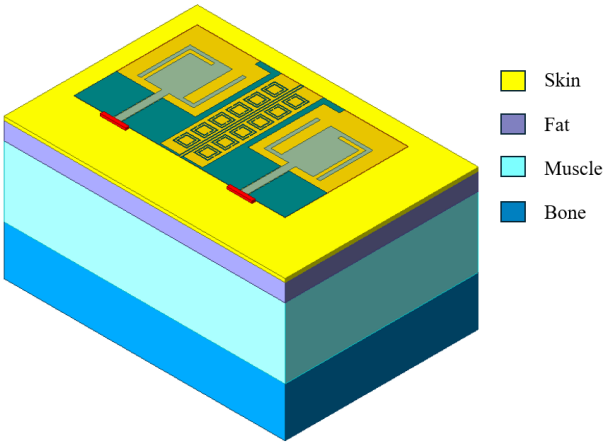

FIGURE 18. Structure of the multi-layer human tissue model used in simulations.

Frequency (GHz)	H (mm)	SAR (W/Kg/10 g)
2.45	3	0.77
	5	0.67
3.45	3	0.90
	5	0.79
6.1	3	1.47
	5	0.93

TABLE 1. SAR values at different spacing heights from the human body model.

TABLE 2. Comparative performance analysis of the proposed antenna and the current literature.

Ref.	Size (mm^3)	Bandwidth (GHz)	Flexible or not	Number of ports	Ground connection	Isolation (dB)	ECC	DG
[5]	$35 \times 33 \times 0.1$	2.4–2.5 (4.08%) 5–7.125 (35%)	YES	1	N/A	N/A	N/A	N/A
[24]	$42 \times 30.5 \times 1.025$	2.28–2.56 (11.57%) 3.28–3.85 (16.0%) 5.06–7.30 (36.2%)	YES	1	N/A	N/A	N/A	N/A
[25]	$56 \times 47 \times 1$	2.15–2.87 (28.69%) 5.13–5.86 (13.28%)	YES	2	YES	> 20	< 0.04	9.99
[29]	$38 \times 28 \times 1.59$	4.04–8.27 (68.7%)	YES	2	YES	> 16	< 0.13	9.99
[26]	$60 \times 60 \times 1$	3.33–3.89 (15.5%)	YES	4	NO	> 15	< 0.01	9.98
[27]	$95 \times 65 \times 0.2$	3.05–3.74 (20.3%)	YES	4	YES	> 15	< 0.1	9.99
[28]	$60 \times 60 \times 0.1$	3.156–3.84 (19.6%) 4.638–6.348 (31.1%)	YES	4	YES	> 21	< 0.12	9.9
[30]	$40 \times 40 \times 1.5$	3.16–4.63 (37.7%) 8.92–12.2 (31.1%)	YES	4	YES	> 20.5	< 0.12	
This work	**$60 \times 34 \times 0.1$**	**1.36–2.71 (66.3%) 3.07–3.655 (17.4%) 4.015–8.245 (68.9%)**	**YES**	**2**	**YES**	**> 20**	**< 0.0012**	**9.999**

antenna on the arm, chest, and thigh. Figure 17 depicts the corresponding S-parameters and the experimental setup for each location. The obtained data validate the antenna's robust performance under on-body conditions, proving its potential for practical wearable applications.

In the simulation model, a human tissue layer structure measuring 55 mm $\times$ 80 mm $\times$ 40 mm was constructed to realistically simulate the influence of biological tissues on antenna performance. The model consists of, from top to bottom: skin (1 mm), fat (5 mm), muscle (20 mm), and bone (14 mm). The overall simulation model is illustrated in Figure 18. Furthermore, the specific absorption rate (SAR) was evaluated at different heights from the human model. The corresponding numerical results are summarized in Table 1, providing key data for assessing the antenna's compliance with human safety regulations. The experimental results indicate favorable SAR performance, meeting the relevant safety standards.

4. COMPARISON

This paper presents a flexible two-port MIMO antenna measuring $60 \times 34 \times 0.1$ mm^3, achieving tri-band operation at 1.36–2.71 GHz, 3.07–3.655 GHz, and 4.015–8.245 GHz, with high isolation (> 20 dB), extremely low envelope correlation coefficient (ECC < 0.0012), and excellent DG close to 10. Compared to existing flexible antenna designs (as summarized in Table 2): although [5] covers the Wi-Fi 7 band (5–7.125 GHz), it

employs a single-port configuration without MIMO capability; [24] is only a wideband single-port flexible antenna; [25, 29] are also flexible two-port designs, and [26–28, 30] are flexible four-port MIMO antennas have good isolation (> 15 dB), yet all of them are single band or dual-band antennas. In summary, while maintaining flexibility, high isolation, ground connection, and a compact footprint, the proposed antenna offers tri-band frequency coverage and superior MIMO performance.

5. CONCLUSION

This paper has successfully developed a compact flexible tri-band dual-element MIMO antenna on a LCP substrate for Wi-Fi 7/5G wireless applications. The measured impedance bandwidths (1.36–2.71 GHz, 3.07–3.655 GHz, and 4.015–8.245 GHz) fully meet the design requirements. The port isolation is better than 20 dB with connected ground. Crucially, the measured MIMO performance metrics are outstanding: an extremely low ECC of < 0.0012, a near-ideal DG of > 9.99999, an MEG difference of < 3 dB, and a TARC below -10 dB across all operating bands, collectively confirming superior MIMO performance and robustness under simultaneous operation. Furthermore, the antenna maintains stable performance when being bent to radii of 30 mm and 50 mm, demonstrating its significant potential as a high-performance flexible solution for next-generation wearable devices.

REFERENCES

[1] Kumar, D., D. Sharma, R. N. Tiwari, I. A. Khan, and P. Kumar, "Multiband flexible MIMO antenna for NB-IoT/ISM/5G and wearable applications," *Results in Engineering*, Vol. 27, 106088, Sep. 2025.

[2] Paşalıoğlu, H., L. Wang, M. Bakır, L. C. Paul, E. Tetik, and M. Karaaslan, "A reconfigurable array and MIMO antenna for 18 GHz and 28/38 GHz applications," *Measurement*, Vol. 257, 118660, Jan. 2026.

[3] Yang, J.-H. and H.-L. Su, "A broadband MIMO antenna array for WiFi-6E/7 in laptop computer applications," in *2024 IEEE International Workshop on Electromagnetics: Applications and Student Innovation Competition (iWEM)*, 1–2, Taoyuan County, Taiwan, Jul. 2024.

[4] Asaad, N. S., A. M. Saleh, and M. A. Alzubaidy, "Analyzing performance of THz band graphene-based MIMO antenna for 6G applications," *Journal of Telecommunications and Information Technology*, Vol. 97, No. 3, 23–29, Sep. 2024.

[5] Nguyen, T. D., S. E. Kim, and C. W. Jung, "Compact, flexible and transparent antenna using MMF for conformal Wi-Fi 7 applications," *Journal of Electrical Engineering & Technology*, Vol. 18, No. 6, 4341–4352, Nov. 2023.

[6] John, D. M., T. Ali, S. Vincent, S. Pathan, J. Anguera, B. Virdee, R. M. David, K. Nayak, and S. P. Gopi, "A dual-band flexible MIMO array antenna for sub-6 GHz 5G communications," *Sensors*, Vol. 25, No. 11, 3557, Jun. 2025.

[7] Desai, A., M. Palandoken, J. Kulkarni, G. Byun, and T. K. Nguyen, "Wideband flexible/transparent connected-ground MIMO antennas for sub-6 GHz 5G and WLAN applications," *IEEE Access*, Vol. 9, 147 003–147 015, 2021.

[8] Tiwari, R. N., D. Sharma, P. Singh, B. G. Kullayappa, P. Kumar, B. R. Swamy, G. P. Kumar, and S. Rajasekaran, "Triple band lateral 4-port flexible MIMO antenna for millimeter wave applications at 24/28/38 GHz," *Results in Engineering*, Vol. 26, 104678, Jun. 2025.

[9] Lee, Y., S.-H. Choi, B.-H. Lee, J.-Y. Lee, and J. H. Kim, "LCP-based low-cost base station antenna for 3.7 GHz 5G band," *Journal of Electromagnetic Engineering and Science*, Vol. 24, No. 3, 276–284, May 2024.

[10] Hu, M., Y. Li, Y. Zhang, P. Wu, and H. Wang, "Ultrathin dual-band circularly polarized antenna," *IEEE Antennas and Wireless Propagation Letters*, Vol. 23, No. 3, 930–934, Mar. 2024.

[11] Peng, H., C. Du, and R. Wang, "Four-port flexible UWB-MIMO antenna with triple band-notched for wearable IoT applications," *International Journal of Microwave and Wireless Technologies*, Vol. 16, No. 8, 1261–1271, Oct. 2024.

[12] Abbasi, N. A., B. Virdee, I. U. Din, S. Ullah, A. A. Althuwayb, N. Rashid, M. Soruri, C. H. See, and M. Alibakhshikenari, "High-Isolation array antenna design for 5G mm-Wave MIMO applications," *Journal of Infrared, Millimeter, and Terahertz Waves*, Vol. 46, No. 1, 12, 2025.

[13] Lodhi, D. and S. Singhal, "CPW fed shovel shaped super wideband MIMO antenna for 5G applications," *AEU — International Journal of Electronics and Communications*, Vol. 168, 154700, Aug. 2023.

[14] Elabd, R. H., A. J. A. Al-Gburi, and A. A. Megahed, "Compact circular MIMO antenna with defected ground structure (DGS) for improved isolation in 5G sub-6 GHz mobile systems," *Results in Engineering*, Vol. 27, 105737, Sep. 2025.

[15] Islam, T., D. Hussain, F. N. Alsunaydih, F. Alsaleem, and K. Alhassoon, "Designing a novel hybrid technique based on enhanced performance wideband millimeter-wave antenna for short-range communication," *Sensors*, Vol. 24, No. 10, 3219, May 2024.

[16] Abhishek, A. and P. Suraj, "Design and analysis of quad port MIMO antenna for mm-Wave and K-band applications using DGS," *Wireless Networks*, Vol. 31, 3705–3726, Jun. 2025.

[17] Tang, Y., T. Wang, J. Zheng, Z. Lyu, X. Tian, and J. Mou, "Mutual coupling suppression of MIMO array with non-uniform curved-strip EBG structure via shape and layout co-optimization," *AEU — International Journal of Electronics and Communications*, Vol. 178, 155306, May 2024.

[18] Wahdiyat, A. I., F. Y. Zulkifli, and E. T. Rahardjo, "Mutual coupling reduction in MIMO antenna using via-less EBG," in *2024 International Symposium on Antennas and Propagation (ISAP)*, 1–2, Incheon, Republic of Korea, Nov. 2024.

[19] Ovelatama, E., U. Umaisaroh, and M. Alaydrus, "Mutual coupling reduction employing rectangular shaped with slotted ring EBG and H-shaped DGS for MIMO antenna," in *2024 IEEE Asia-Pacific Microwave Conference (APMC)*, 435–437, Bali, Indonesia, Nov. 2024.

[20] Galib, S. N. and S. V. A.-D. Makki, "High-performance eight-port MIMO antenna for sub-6 GHz 5G smartphones," *International Journal of Intelligent Engineering & Systems*, Vol. 17, No. 6, 312, 2024.

[21] Godi, R. C. and R. R. Patil, "SRA-DGS-NL based decoupling scheme for MIMO antenna," *Progress In Electromagnetics Research C*, Vol. 148, 1–7, 2024.

[22] Rath, S., G. Palai, and S. K. L., "A penta-band CSRR loaded dielectric resonator antenna for X-band, W-LAN, Wi-Fi 6, and Wi-Max applications," *Optical and Quantum Electronics*, Vol. 56, No. 8, 1374, Aug. 2024.

[23] Patil, U. A., A. B. Kakade, and A. U. Patil, "Low cross-polarization high-isolation 2-element MIMO antenna for unmanned aerial vehicle," *AEU — International Journal of Electronics and Communications*, Vol. 177, 155164, Apr. 2024.

[24] Ye, D., H. Zu, Z. Hu, Y. Xin, J. Guo, R. Song, and D. He, "Flexible and compact tri-band graphene antenna for conformal Wi-Fi/WiMAX/5G applications," *IEEE Transactions on Circuits and Systems II: Express Briefs*, Vol. 71, No. 3, 1086–1090, Mar. 2024.

[25] Roy, A., A. K. Biswas, A. Nandi, and B. Basu, "A compact flexible wide band-notched UWB MIMO antenna with very high decoupling characteristics for WLAN applications," *Wireless Personal Communications*, Vol. 140, 659–683, Jan. 2025.

[26] Sundaravadivel, P., M. R. Raja, C. Annadurai, and D. R. Kumar, "A novel moon-shaped flexible four-element co-planar antenna for 5G applications," *Optical and Quantum Electronics*, Vol. 56, No. 10, 1612, Sep. 2024.

[27] Kulkarni, N., R. M. Linus, and N. B. Bahadure, "A small wideband inverted l-shaped flexible antenna for sub-6 GHz 5G applications," *AEU — International Journal of Electronics and Communications*, Vol. 159, 154479, Feb. 2023.

[28] Zhang, J., C. Du, L. Pei, and H. Liu, "A CPW-fed dual band four-port MIMO antenna based on liquid crystal polymer for flexible IoT applications," *International Journal of Microwave and Wireless Technologies*, Vol. 15, No. 9, 1570–1578, Nov. 2023.

[29] Alekhya, B., A. Lokam, and S. Modak, "Textile based loaded annular ring MIMO antenna system for wearable 5G applications in the Sub-6 GHz band," *AEU — International Journal of Electronics and Communications*, Vol. 198, 155851, Aug. 2025.

[30] Biswas, A. K., S. Biswas, S. Haldar, and A. Nandi, "A highly decoupled flexible 4-element MIMO antenna with band notched characteristics for ultra wide-band wearable applications," *AEU — International Journal of Electronics and Communications*, Vol. 173, 154985, Jan. 2024.